Non-Oberbeck-Boussinesq Effects in Rayleigh-Bénard Convection of Liquids

Susanne Horn, Olga Shishkina, and Claus Wagner

Abstract. The influence of temperature-dependent material properties on Rayleigh–Bénard convection is investigated in three different liquids, ranging from a very small Prandtl number for mercury with $Pr = 0.0232$, over a moderate one for water with $Pr = 4.38$, to a very large one for glycerol with $Pr = 2548$. For this purpose, three-dimensional direct numerical simulations were performed in a cylindrical cell with a unity aspect ratio. Local quantities such as the viscous and thermal boundary layer thicknesses, the centre temperature and the wind velocity show a breakdown of the top-bottom symmetry. The intensity of this asymmetry strongly depends on the respective fluid.

1 Introduction

Thermal convection is one of the most fundamental problems in geo- and astrophysics. Examples to mention here are the convection in the outer layer of stars, in the Earth's atmosphere and oceans or the mantle convection on Earth and other rocky planets. Furthermore, it is also important for engineering applications. Examples here are crystal growth or the air flow in aircraft cabins. However, the physical process itself is still not completely understood. Thus, the idealised scenario, i.e. a fluid heated from below and cooled from above, the so-called Rayleigh-Bénard convection, has received ongoing attention for over a century now.

For theoretical and numerical investigations commonly the classical Oberbeck-Boussinesq (OB) approximation is employed. That means, the fluid is considered to be incompressible and all material properties are constant with respect to the pressure and the temperature. The only exception is the density, which varies linearly with the temperature. However, the validity range of this approach is often very

Susanne Horn · Olga Shishkina · Claus Wagner
German Aerospace Center, Institute for Aerodynamics and Flow Technology,
Göttingen, Germany
e-mail: susanne.horn@dlr.de

M.O. Deville et al. (eds.), *Turbulence and Interactions*,
Notes on Numerical Fluid Mechanics and Multidisciplinary Design 125,
DOI: 10.1007/978-3-662-43489-5_12,

restrictive and deviations due to the violation of the OB assumption are referred to as non-Oberbeck-Boussinesq (NOB) effects. NOB effects in gases are mostly induced by compressibility and the pressure dependence of the material properties. On the contrary, in liquids the temperature dependence is crucial for NOB effects. This is what we will focus on in the following. As a step in the direction to predict the flow behaviour of realistic fluids, we study the influence of temperature-dependent material properties in liquids by means of Direct Numerical Simulations (DNS).

2 Validity Range of the OB Approximation

A rigorous mathematical deduction for the validity range of the OB approximation was given by Gray & Giorgini [1]. In short, it states that if certain ε_i are smaller than a requested accuracy, e.g. 0.1, a residual error of at most 10 % is guaranteed.

$$\varepsilon_1 = \frac{\alpha_m g H}{c_{p,m}} \frac{T_m}{\Delta},\ \varepsilon_2 = \frac{\alpha_m g H}{c_{p,m}} \frac{\nu_m}{\kappa_m},\ \varepsilon_3 = -\frac{\Delta}{\rho_m} \frac{\partial \rho}{\partial T}\bigg|_{T_m},\ \varepsilon_4 = \frac{\Delta}{c_{p,m}} \frac{\partial c_p}{\partial T}\bigg|_{T_m}, \tag{1}$$
$$\varepsilon_5 = \frac{\Delta}{\rho_m \nu_m} \frac{\partial(\rho\nu)}{\partial T}\bigg|_{T_m},\ \varepsilon_6 = \frac{\Delta}{\Lambda_m} \frac{\partial \Lambda}{\partial T}\bigg|_{T_m},\ \varepsilon_7 = \frac{\Delta}{\alpha_m} \frac{\partial \alpha}{\partial T}\bigg|_{T_m}.$$

Here T is the temperature, H the height of the Rayleigh–Bénard cell, g the gravitational acceleration, α the isobaric expansion coefficient, ρ the density, ν the kinematic viscosity, Λ the heat conductivity, c_p the specific heat at constant pressure and $\Delta = T_b - T_t$ the imposed adverse temperature difference. The indices t, b and m refer to the quantity at the top, the bottom and the arithmetic mean temperature $T_m = (T_t + T_b)/2$, respectively.

We exemplarily applied their method to three different liquids, which significantly distinguish themselves through their different Prandtl numbers, $Pr = \nu_m/\kappa_m$. Namely, glycerol with $Pr = 2548$ (figure 1(a)), water with $Pr = 4.38$ (figure 1(b))

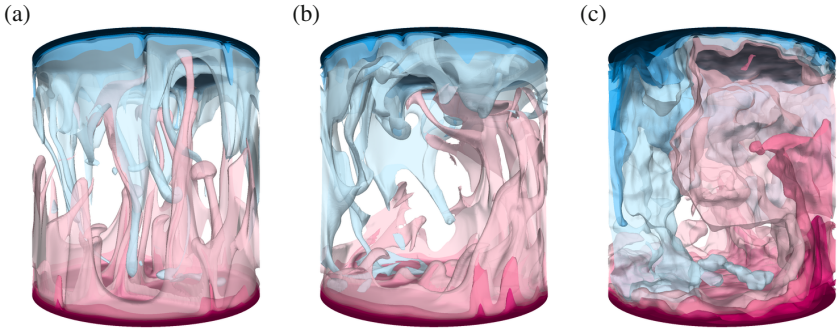

Fig. 1 Instantaneous flow fields for (a) glycerol ($Pr = 2548$), (b) water ($Pr = 4.38$) and (c) mercury ($Pr = 0.0232$) for $Ra = 10^8$ under OB conditions, obtained by DNS on a $N_r \times N_\phi \times N_z = 192 \times 512 \times 384$ mesh. Shown are ten temperature isosurfaces equidistantly distributed between the top and bottom temperature.

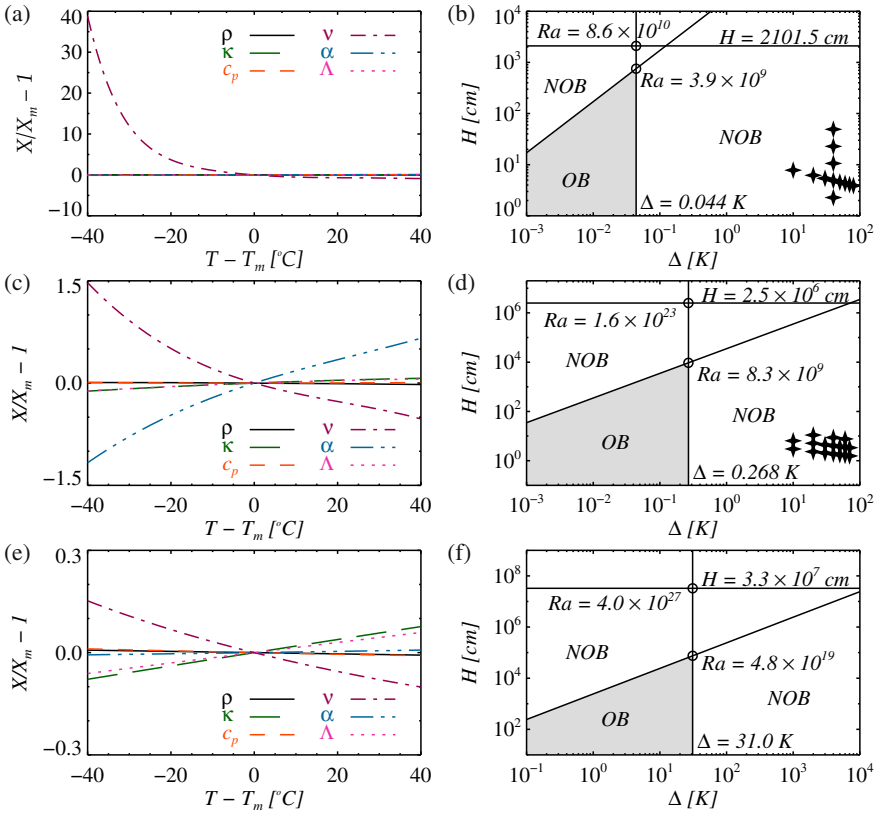

Fig. 2 Material properties $X \in \{\rho, \kappa, c_p, \nu, \alpha, \Lambda\}$ for (a) glycerol, (c) water and (e) mercury. The corresponding regions of validity of the Oberbeck–Boussinesq approximation for (b) glycerol, (d) water and (f) mercury at $T_m = 40\,°\mathrm{C}$, according to Gray & Giorgini [1]. The grey shaded areas show the parameter range where the OB assumption is valid. The stars denote our NOB DNS parameters.

and mercury with $Pr = 0.232$ (figure 1(c)). The material properties of each fluid [2, 3, 4] are shown in figure 2(a), (c) and (e), respectively. Glycerol only exhibits a strongly temperature-dependent viscosity, while all the other thermophysical properties are virtually constant. This suggests that NOB effects occur already at small Δ. Indeed, the validity range diagram according to Gray & Giorgini [1], presented in figure 2(b), confirms it, showing that the maximal admissible temperature difference is $\Delta = 0.044\,\mathrm{K}$. It also shows that the maximal attainable Rayleigh number $Ra = \alpha_m g \Delta H^3/(\kappa_m \nu_m)$ under OB conditions is 3.9×10^9. For water, the variation of the material properties is much weaker, however, the variation in ν and α is of the same strength, and also the variation in Λ and κ, respectively, is not negligible. The validity range presented in figure 2(d) shows that OB conditions are limited to $\Delta < 0.268\,\mathrm{K}$. Finally, mercury has almost constant material properties, and thus

NOB factors are only to be expected for larger Δ (figure 2(f)). Since our objective is the investigation of NOB effects, we will concentrate on water and glycerol.

3 Numerical Method

For our studies of Rayleigh–Bénard convection we perform DNS with a well-tested fourth order accurate finite volume code for cylindrical domains. The code is based on `flowsi`, originally developed by Schmitt & Friedrich [5]. It solves the Navier–Stokes equations on staggered grids and uses the volume balance procedure motivated by Schumann [6]. Later on, it was advanced with a fourth order accurate spatial integration scheme and for the simulation of Rayleigh–Bénard convection by Shishkina & Wagner [7]. For the purpose of investigating NOB effects, we implemented temperature-dependent material properties, adopted from Ahlers et al. [2] and Segur & Oberstar [3]. The viscosity ν, the heat conductivity Λ, the diffusivity κ and the density ρ in the buoyancy term are described by polynomials up to third order in the case of water and up to seventh order in the case of glycerol. Hence, we solve

$$\frac{1}{r}\partial_r(ru_r) + \frac{1}{r}\partial_\phi u_\phi + \partial_z u_z = 0, \tag{2}$$

$$\begin{aligned} D_t u_r - \frac{u_\phi^2}{r} + \frac{1}{\rho_m}\partial_r p &= \frac{1}{r}\partial_r\left(r\nu\tilde{\tau}_{rr}\right) + \frac{1}{r}\partial_\phi\left(\nu\tilde{\tau}_{r\phi}\right) + \partial_z\left(\nu\tilde{\tau}_{rz}\right) - \frac{1}{r}\nu\tilde{\tau}_{\phi\phi}, \\ D_t u_\phi + \frac{u_r u_\phi}{r} + \frac{1}{\rho_m}\frac{1}{r}\partial_\phi p &= \frac{1}{r^2}\partial_r\left(r^2\nu\tilde{\tau}_{\phi r}\right) + \frac{1}{r}\partial_\phi\left(\nu\tilde{\tau}_{\phi\phi}\right) + \partial_z\left(\nu\tilde{\tau}_{\phi z}\right), \\ D_t u_z + \frac{1}{\rho_m}\partial_z p &= \frac{1}{r}\partial_r\left(r\nu\tilde{\tau}_{zr}\right) + \frac{1}{r}\partial_\phi\left(\nu\tilde{\tau}_{z\phi}\right) + \partial_z\left(\nu\tilde{\tau}_{zz}\right) + \frac{\rho_m-\rho}{\rho_m}g, \end{aligned} \tag{3}$$

$$\rho_m c_{p,m} D_t T = \frac{1}{r}\partial_r(\Lambda r\partial_r T) + \frac{1}{r^2}\partial_\phi(\Lambda\partial_\phi T) + \partial_z(\Lambda\partial_z T). \tag{4}$$

Here D_t denotes the material derivative, p the pressure and u_r, u_ϕ, u_z the radial, azimuthal and vertical velocity component, respectively. The tensor $\tilde{\tau}$ is defined as $\tilde{\tau} = \tau/(\rho_m\nu)$, with τ being the deviatoric stress tensor. All other variables have their usual meaning and were already introduced in the previous section.

4 Results and Discussion

The main feature of Rayleigh-Bénard convection under NOB conditions is the breakdown of the top-bottom symmetry, found under OB conditions. This can be realised at first glance by comparing figure 1 and 3. Thus, one of the objectives of NOB studies is to understand and quantify these asymmetries.

The probably best analysed NOB characteristic is the deviation of the centre temperature T_c from the arithmetic mean temperature T_m, as depicted in figure 4. For $\Delta = 70\,\mathrm{K}$, we obtain a T_c that is 11.9 K higher than T_m in the case of glycerol, whereas in contrast, in the case of water the observed increase of T_c is only about 5.6 K. The reason lies in the different viscosities in the cold top and hot bottom layer. That is, the lower viscosity at the warm bottom makes the plumes more mobile, i.e. faster. The cold plumes from the top show the exact opposite behaviour,

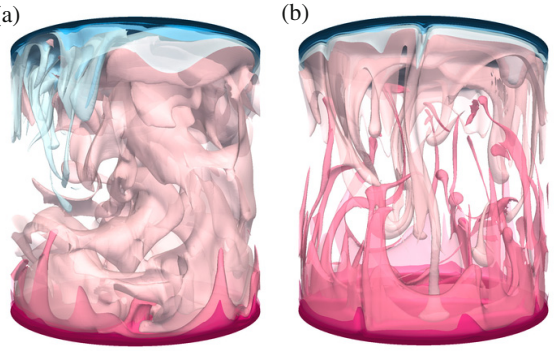

Fig. 3 Instantaneous flow fields (a) water and (b) glycerol for $Ra = 10^8$ under NOB conditions ($\Delta = 40\,\mathrm{K}$). Shown are ten temperature isosurfaces equidistantly distributed between the top and bottom temperature.

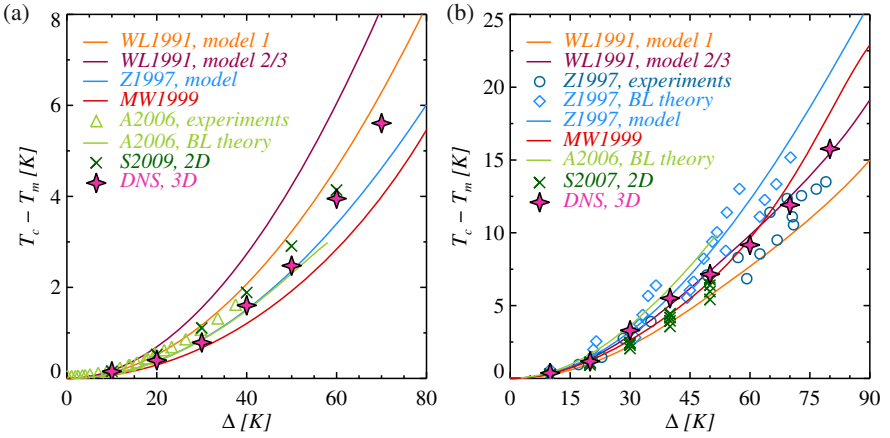

Fig. 4 Comparison of the centre temperature T_c as function of Δ for (a) water and (b) glycerol obtained by our three-dimensional DNS with models by Wu & Libchaber [8] (WL1991), Zhang et al. [9] (Z1997), Manga & Weeraratne [10] (MW1999) and Ahlers et al. [2] (A2006). Additionally, experimental data by Ahlers et al. [2] and Zhang et al. [9], and results from two-dimensional simulations by Sugiyama et al. [11, 12] (S2007, S2009) are shown.

i.e. they are very viscous and move much slower. Hence, they are much longer in contact with the ambient medium in the bulk and heat up on their way down. Thus, the much stronger viscosity dependence in glycerol leads to a significantly higher T_c than observed in water. Several models exist to predict T_c, either based on the Prandtl-Blasius boundary layer theory or on classical scaling theories, see Horn et al. [13] for details. These theories work differently well for a particular fluid.

The asymmetric plume dynamics are also reflected in the velocity profiles. In figure 5 the specific kinetic energy

$$U^E = \sqrt{\tfrac{1}{2}\left(u_r^2 + u_\phi^2 + u_z^2\right)} \tag{5}$$

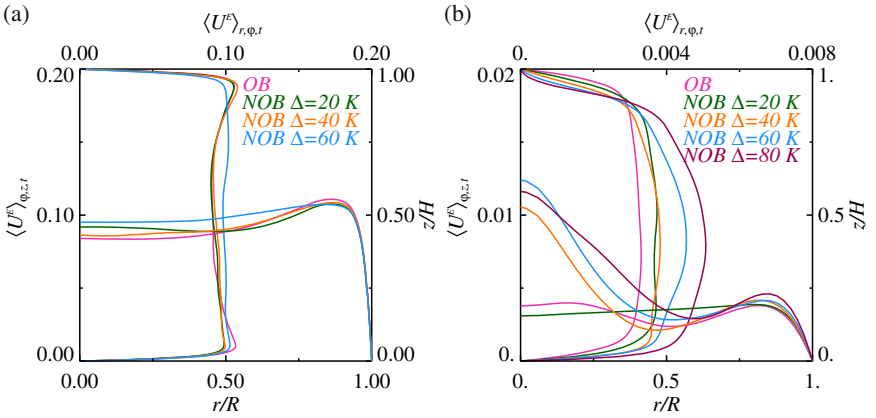

Fig. 5 Specific kinetic energy normalised by the buoyancy velocity $\sqrt{g\alpha_m R\Delta}$ for (a) water and (b) glycerol. The profiles are averaged in time and radial and azimuthal direction and shown as function of the vertical coordinate z/H, as well as averaged in time and the azimuthal and vertical direction as function of the radial coordinate r/R.

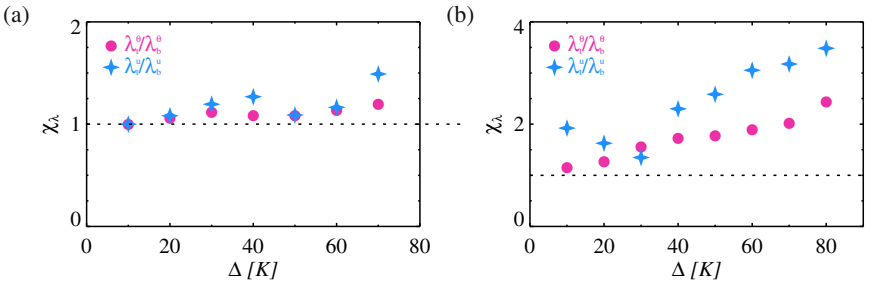

Fig. 6 Ratio of the thermal top and bottom boundary layers, $\chi_{\lambda^\theta} = \lambda_t^\theta/\lambda_b^\theta$, and the viscous ones, $\chi_{\lambda^u} = \lambda_t^u/\lambda_b^u$ as function of Δ for (a) water and (b) glycerol

is presented. While for water (figure 5(a)) a difference is only hardly visible between the OB and NOB profiles, the NOB profiles for glycerol (figure 5(b)) are clearly bended away from the plate at the top and towards the plate at the bottom. This bending increases with Δ.

In line with this, the top viscous boundary layer λ_t^u is always thicker than the bottom one λ_b^u, defined as

$$\lambda_t^\theta = \left(\frac{\partial\langle T\rangle_{r,\phi,t}}{\partial z}\bigg|_t\right)^{-1}(T_t - T_c), \qquad \lambda_b^\theta = \left(\frac{\partial\langle T\rangle_{r,\phi,t}}{\partial z}\bigg|_b\right)^{-1}(T_c - T_b). \tag{6}$$

The same is true for the thermal boundary layers,

$$\lambda_t^u = \max\left(z|_{\frac{\partial\langle u_{r,rms}\rangle}{\partial z}=0}\right), \qquad \lambda_b^u = \min\left(z|_{\frac{\partial\langle u_{r,rms}\rangle}{\partial z}=0}\right), \tag{7}$$

as seen in figure 6. However, this behaviour is non-linear with Δ and in the case of glycerol, this leads to different coherent flow structures [13].

5 Concluding Remarks

A series of three-dimensional DNS has been conducted to study the effects of temperature-dependent material properties in real liquids by considering the examples of water and glycerol. Our simulations revealed that NOB effects lead to a breakdown of the top-bottom symmetry typical for OB simulations. The observed NOB effects include, but are not limited to, different thermal and viscous boundary layer thicknesses, asymmetric plume dynamics and an increase of T_c. Their intensity strongly depends on the particular fluid.

Acknowledgements. The authors acknowledge support by the *Deutsche Forschungsgemeinschaft (DFG)* under grant SH405/2-1.

References

[1] Gray, D.D., Giorgini, A.: Int. J. Heat Mass Transfer 19 (1976)
[2] Ahlers, G., Brown, E., Fontenele Araujo, F., Funfschilling, D., Grossmann, S., Lohse, D.: JFM 569 (2006)
[3] Segur, J.B., Oberstar, H.E.: Ind. Eng. Chem. 43 (1951)
[4] International Atomic Energy Agency, Vienna, Thermophysical properties of materials for nuclear engineering: A tutorial and collection of data (2008)
[5] Schmitt, L., Friedrich, R.: 7th GAMM-Conference on Numerical Methods in Fluid Mechanics. Vieweg und Sohn (1988)
[6] Schumann, U.: J. Comput. Phys. 18(4) (1975)
[7] Shishkina, O., Wagner, C.: C. R. Mécanique 333 (2005)
[8] Wu, X.Z., Libchaber, A.: Phys. Rev. A 43(6) (1991)
[9] Zhang, J., Childress, S., Libchaber, A.: Phys. Fluids 9(4) (1997)
[10] Manga, M., Weeraratne, D.: Phys. Fluids 11(10) (1999)
[11] Sugiyama, K., Calzavarini, E., Grossmann, S., Lohse, D.: EPL 80 (2007)
[12] Sugiyama, K., Calzavarini, E., Grossmann, S., Lohse, D.: JFM 637 (2009)
[13] Horn, S., Shishkina, O., Wagner, C.: J. Fluid Mech. 724, 175 (2013)